


NANO EXPRESS

Open Access



Green Synthesized Phytochemically (*Zingiber officinale* and *Allium sativum*) Reduced Nickel Oxide Nanoparticles Confirmed Bactericidal and Catalytic Potential

Ali Haider¹, Muhammad Ijaz^{1*}, Sidra Ali², Junaid Haider³, Muhammad Imran⁴, Hamid Majeed⁵, Iram Shahzadi⁶, Muhammad Muddassir Ali⁷, Jawaria Ali Khan¹ and Muhammad Ikram^{8*} 

Abstract

Phyto-synthesized nanoparticles (NPs) having reduced chemical toxicity have been focused globally and become essential component of nanotechnology recently. We prepared green phytochemically (ginger and garlic) reduced NiO-NPs to replace synthetic bactericidal and catalytic agent in textile industry. NPs were characterized using ultra-violet visible spectroscopy (UV-Vis), X-ray diffraction (XRD), X-ray photoelectron spectroscopy (XPS), Fourier-transform infrared spectroscopy (FTIR), energy-dispersive X-ray spectroscopy (EDS), scanning electron microscopy (SEM), and transmission electron microscopy (TEM). The synthesis of NPs was confirmed by XRD and UV-Vis having strong absorption at 350 nm with size ranged between 16–52 nm for ginger and 11–59 nm for garlic. Scanning and transmission electron microscopy confirmed pleomorphism with cubic- and more spherical-shaped NPs. Moreover, exact quantities of garlic and ginger extracts (1:3.6 ml) incorporated to synthesize NiO-NPs have been successfully confirmed by FTIR. Phytochemically reduced NPs by garlic presented enhanced bactericidal activity against multiple drug-resistant *Staphylococcus aureus* at increasing concentrations (0.5, 1.0 mg/50 μ l) and also degraded methylene blue (MB) dye efficiently. Conclusively, green synthesized NiO-NPs are impending activists to resolve drug resistance as well as environment friendly catalytic agent that may be opted at industrial scale.

Keywords: Metal oxide, Particle size, Diseases

Introduction

Nanotechnology matter influence with at least one dimension size 1–100 nm that provides ability to engineer material by controlling their size [17]. NPs due to their unique chemical, physical, and biological properties in various fields, including medicine, have attained great

attention. Their properties can be easily altered by changing size at nanometer scale [47].

Nickel (Ni) and nickel oxide (NiO) NPs have great importance due to their particular magnetic, catalytic, and electronic properties in energy technology, magnetism, biomedicines, and electronics [9, 26, 35]. NiO with a wide band gap of 3.6 to 4.0 eV and cubic lattice structure has potential due to p-type semiconductor. These NPs having high chemical stability, super capacitance properties, electron transfer capability, and electro catalysis are being used in biomedicines and photocatalytic, anti-inflammatory, and antibacterial activities [8, 10, 11, 45].

* Correspondence: mijaz@uvas.edu.pk; dr.muhammadikram@gcu.edu.pk

¹Department of Clinical Medicine and Surgery, University of Veterinary and Animal Sciences, Lahore, Punjab 54000, Pakistan

⁸Solar Cell Applications Research Lab, Department of Physics, Government College University, Lahore, Punjab 54000, Pakistan

Full list of author information is available at the end of the article

The emergence of infectious maladies, especially antibiotic-resistant (MDR), has devastated public health worldwide. Generally, both pathogenic Gram-positive (G +ve) and Gram-negative (G -ve) bacterial strains are among major public health threats.

In dairy industry, bovine mastitis is a major problematic disease having great economic impact characterized by chemical, microbiological, and physical changes in milk, while pathological changes in udder glandular tissues [6, 19]. Mastitis etiology includes infectious agents, i.e., bacteria, viruses, and fungi and most important are bacteria, divided into two groups: major (*Streptococci*, *Staphylococcus aureus*, *Corynebacterium pyogenes*, and *Coliform*) and minor pathogens (*Corynebacterium bovis* and *coagulase-negative Staphylococci*) [25]. The emergence of multiple drug-resistant Gram-positive and Gram-negative bacterial strains poses significant threat to public health [23, 32].

Zingiber officinale (ginger) is an important ingredient in Ayurvedia and Unani, and Chinese herbal medicine is treated for various ailments such as anti-nausea, digestive aid, rheumatism, and bleeding disorders due to wide diversity of volatile oils like zingiberol, monoterpene, sesquiterpene, and sesquiterpene hydrocarbons [12, 13, 43]. However, *Allium sativum* (garlic) contain organo-sulfur components, i.e., allyl sulphide groups, alliin, ajoene, allyl cysteine and allicin, and others such as vitamins, phospholipids, flavonoids, amino acids, and fatty acids that orient its medical properties [14, 24]. We aimed to assess bactericidal action of phytochemically reduced Ni metal oxide

NPs against MDR (*S. aureus*), an isolate of bovine mastitis, and this will be the first report from Pakistan in veterinary research area on above mentioned agent.

Methods

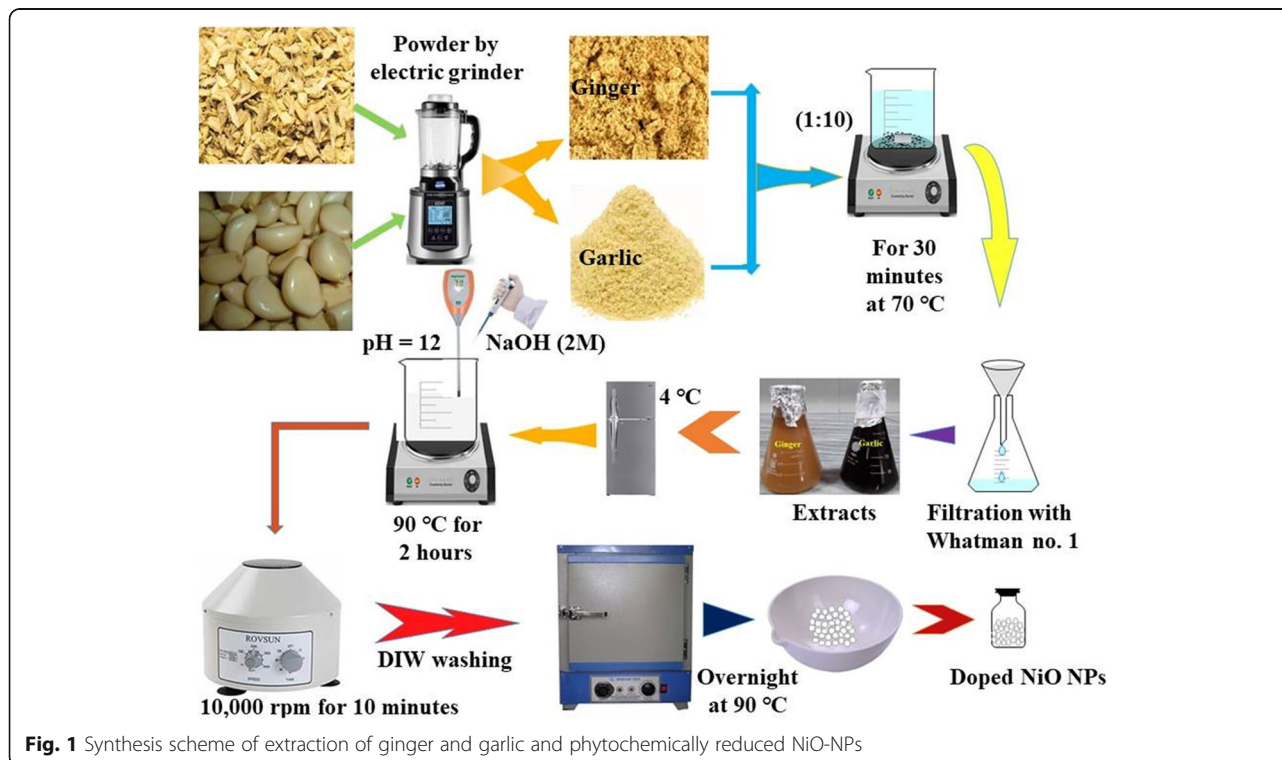
The current study was aimed at investigating the bactericidal action of phytochemically reduced NiO-NPs against MDR (*S. aureus*), an isolate of bovine mastitis.

Materials

Nickel nitrate [$\text{Ni}(\text{NO}_3)_2$], sodium hydroxide (NaOH), methylene blue (MB), and sodium borohydride (NaBH_4) of analytical grade were purchased from Sigma-Aldrich®, and fresh ginger and garlic roots were collected from the local market. Roots were dried in shade to achieve constant weight for further processing. Antibiotic discs were purchased from Bioanalyse® (Turkey). Bacterial growth media used were of analytical grade by TM Media, (Titan Biotech Ltd, India).

Preparation of Aqueous Extracts

Ginger and garlic roots were pulverized to fine dust by using electric grinder and preserved in plastic containers. Grounded root's powder were mixed with controlled quantity of distilled water-DIW (1:10) under vigorous stirring at 70 °C for 30 min. Extracts were cooled, filtered by Whatman No.1 filter paper, and stored at 4 °C (Fig. 1) till further use.



Green Synthesis of NiO-NPs

Ginger and garlic aqueous extracts of various ratios (1.2, 1.8, 2.4, 3.0, 3.6, and 4.2 ml) were added to nickel nitrate (0.1 M) under continuous stirring. Stirred solution pH 12 was maintained using NaOH (2 M) at 90 °C for 2 h. The precipitates formed were centrifuged at 10,000 rpm for 10 min, washed with DIW, and were dried overnight in hot air oven at 90 °C illustrated in Fig. 1.

Characterization

Absorption maxima (λ_{max}) of synthesized NPs were scanned by UV-Visible spectrophotometer (Genesys 10 S) from 200–800 nm wavelengths. Phase composition and structural information were analyzed by X-ray diffraction (XRD) BUNKER D2 phaser having 2 θ range of (10–80°) equipped with Cu K α 1 radiations of $\lambda = 1.540 \text{ \AA}$. Green synthesized NiO-NP functional

groups were recorded using Fourier-transform infrared spectroscopy (ATR-FTIR). Size, shape, and elemental analysis of NPs were analyzed by field emission electron microscope (FESEM) and transmission electron microscopy Hitachi H7100FA (TEM). The sample composition with corresponding band gaps were investigated by X-ray photoelectron spectroscopy (XPS).

Isolation and Identification of MDR *S. aureus*

Isolation of *S. aureus*

Clinically positive bovine milk samples collected from private and public sector veterinary hospitals and farms in Punjab, Pakistan, were cultured upon 5% sheep blood agar and incubated at 37 °C for 24–48 h. The characteristic colonies obtained were further streaked on mannitol salt agar (MSA) TM Media

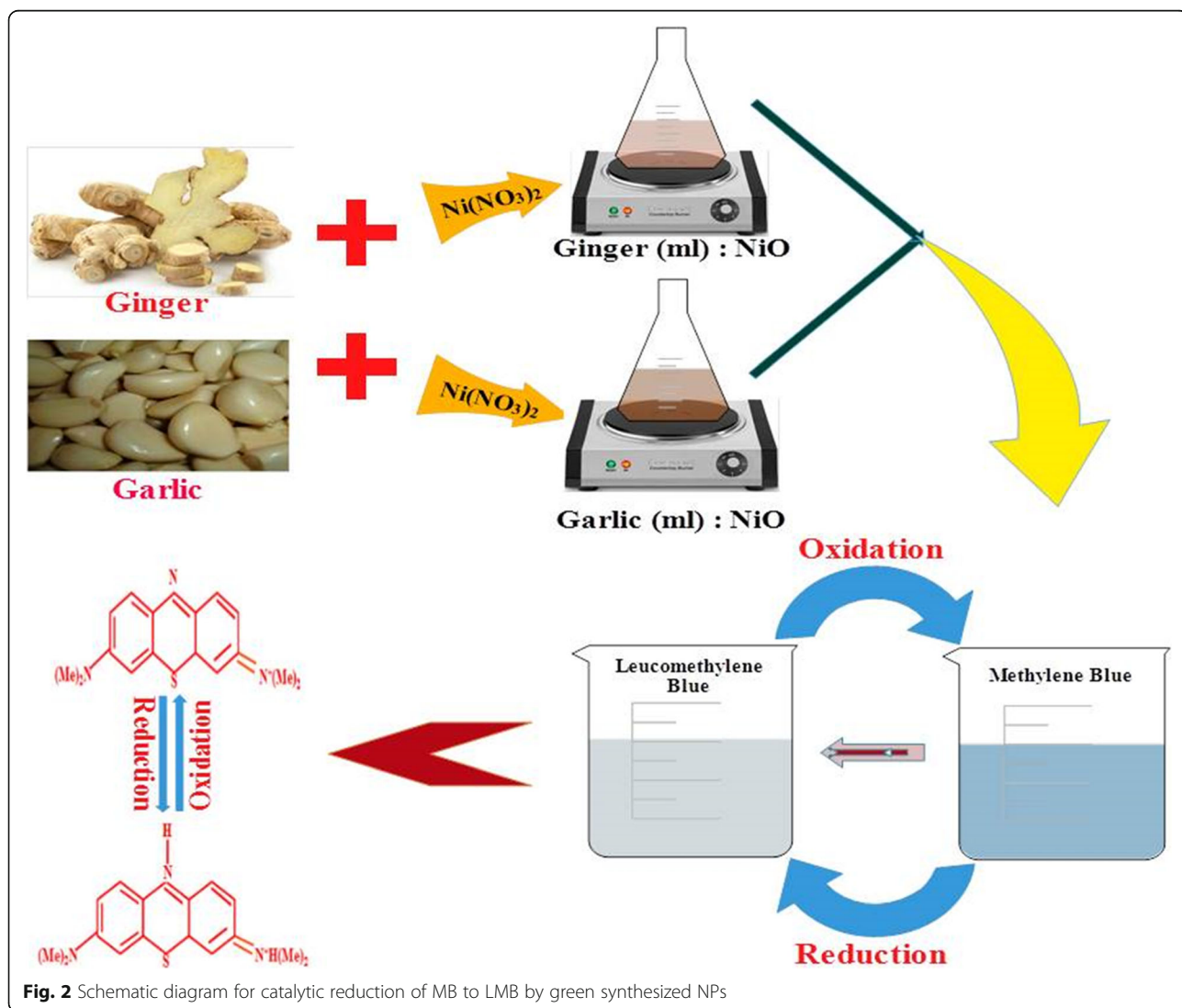


Fig. 2 Schematic diagram for catalytic reduction of MB to LMB by green synthesized NPs

(Titan Biotech Ltd, India) in triplets to isolate purified *S. aureus*.

Identification of MDR *S. aureus*

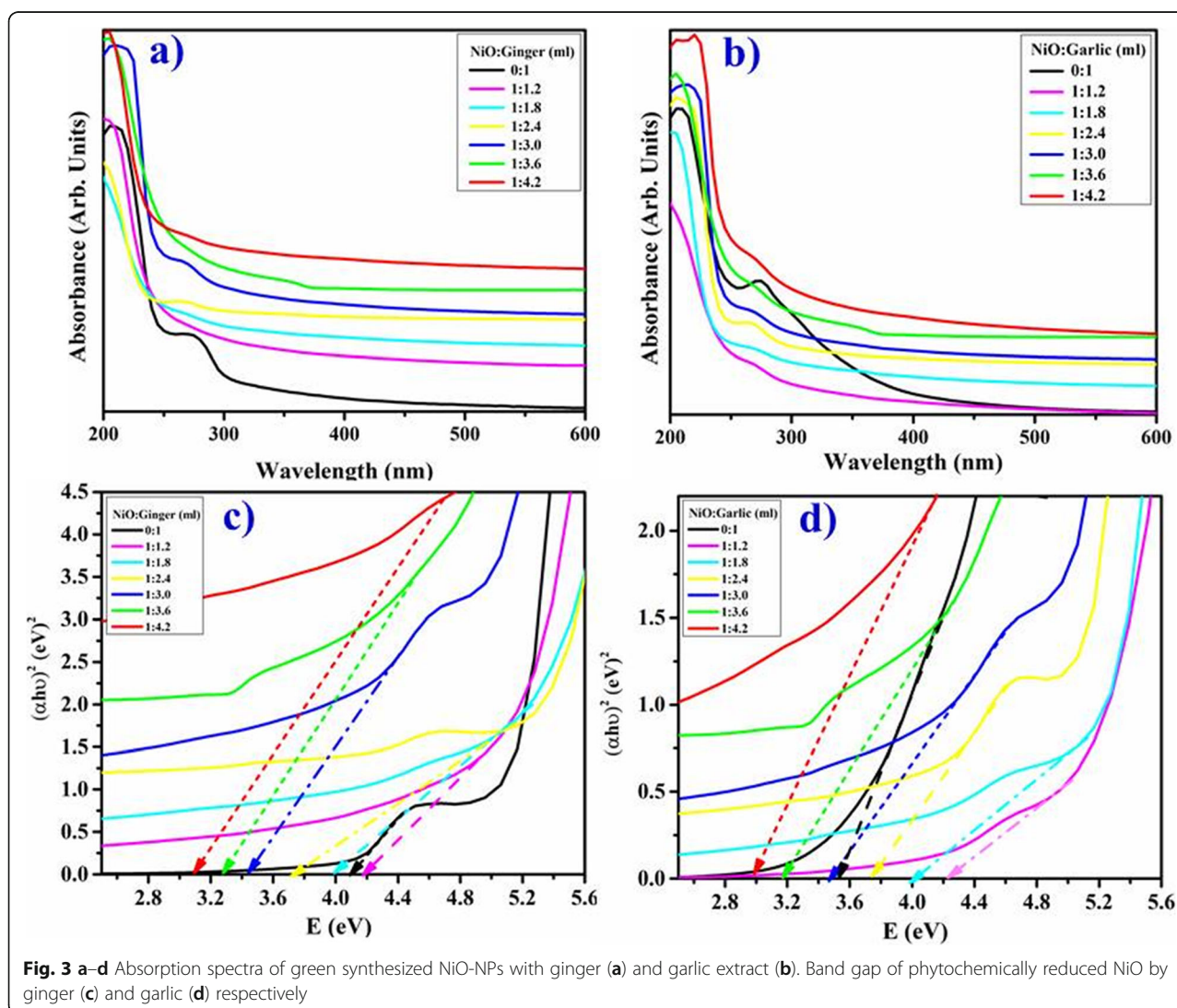
Identification of bacterial colonies was done through morphological characteristics, Gram's staining, and biochemical procedures (coagulase and catalase test) as per description of Burgey's manual of determinative bacteriology.

Antibiotic susceptibility of characteristic colonies was evaluated by disk diffusion test based upon guidelines of National Committee for Clinical Laboratory Standards (NCCLS) for isolation of MDR *S. aureus*. Antibiotic discs containing oxytetracycline (30 μg), tylosine (30 μg), gentamicin (10 μg), ciprofloxacin (5 μg), and trimethoprim + sulphamethoxazole (1.25 μg + 23.75 μg) applied aseptically on Mueller-Hinton agar (MHA) TM Media (Titan Biotech Ltd, India) 1×10^8 CFU/ml were kept at

37 °C for 24 h [7]. Bacterium found resistant to minimum three antibiotics was declared MDR [28].

Antimicrobial Activity

In vitro antimicrobial action potential of phytochemically reduced NiO-NPs was evaluated by agar well diffusion method upon ten representative isolates of MDR *S. aureus* collected from mastitic milk. Petri dishes were swabbed with 1.5×10^8 CFU/ml (0.5 McFarland standard) MDR *S. aureus* on MSA. Wells of 6 mm diameter were formed using sterile cork borer. Various concentrations of individual aqueous extracts of ginger, garlic, and green synthesized (phytochemically reduced) NiO-NPs were applied. Aqueous extracts were used at concentrations of (10 mg/100 μl) and (50 mg/100 μl) and NiO (0.5 mg/50 μl) and (1.0 mg/50 μl). Ciprofloxacin (0.005 mg/50 μl) was used



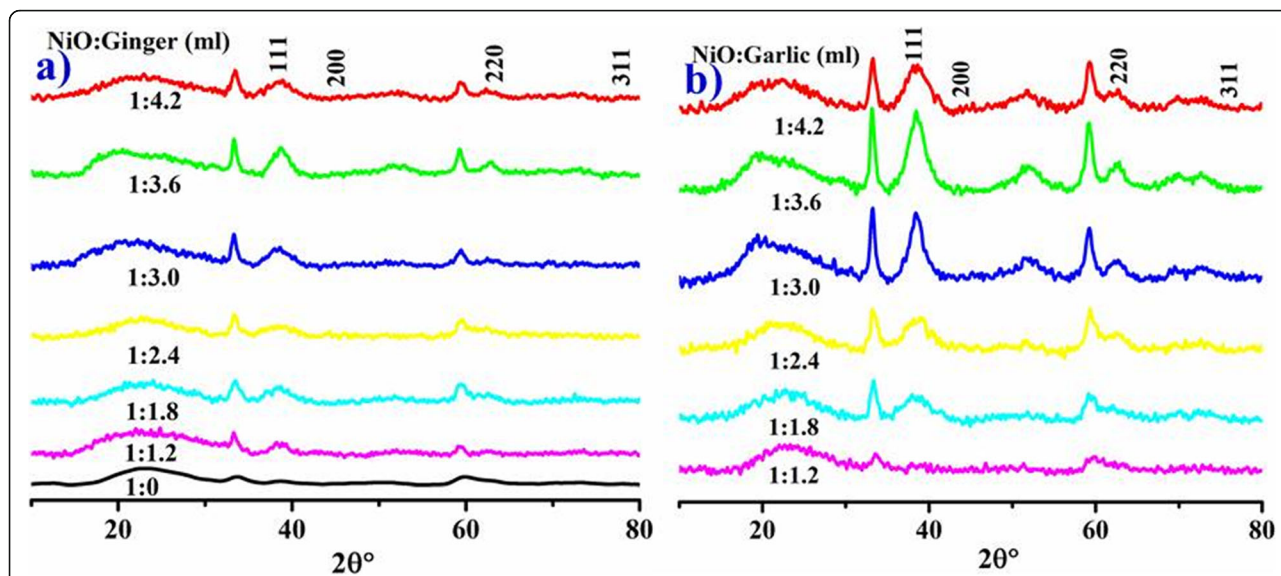


Fig. 4 XRD pattern of different concentrations of phytochemically reduced NiO by ginger (a) and garlic (b) and standard NiO (c)

as positive control and DIW as negative control (50 µl).

Statistical Analysis

The antimicrobial efficacy was calculated in terms of inhibition zone (mm) size, and inhibition zone diameters were analyzed statistically by one-way analysis of variance (ANOVA) using SPSS 20.

Catalysis

For catalytic evaluation of synthesized extract NiO, freshly prepared aqueous sodium borohydride (300 µl) was mixed with 3 ml methylene blue (0.03×10^{-3} M)

solution. Subsequently, 300 µl colloidal sample of desired concentration was added to solutions. Light blue color of methylene blue dye (MB) disappeared representing dye degradation to leucomethylene blue as shown in Fig. 2. The absorption was noted between 200–800 nm using UV-Vis spectrophotometer.

Results and Discussion

Optical properties of phytochemically reduced NiO by ginger and garlic aqueous extracts between 200–600 nm are presented in Fig. 3a, b. The maximum absorbance (λ_{max}) in NiO-NPs was observed around 350 nm (1:3.6 ml) which increased with extracts concentration

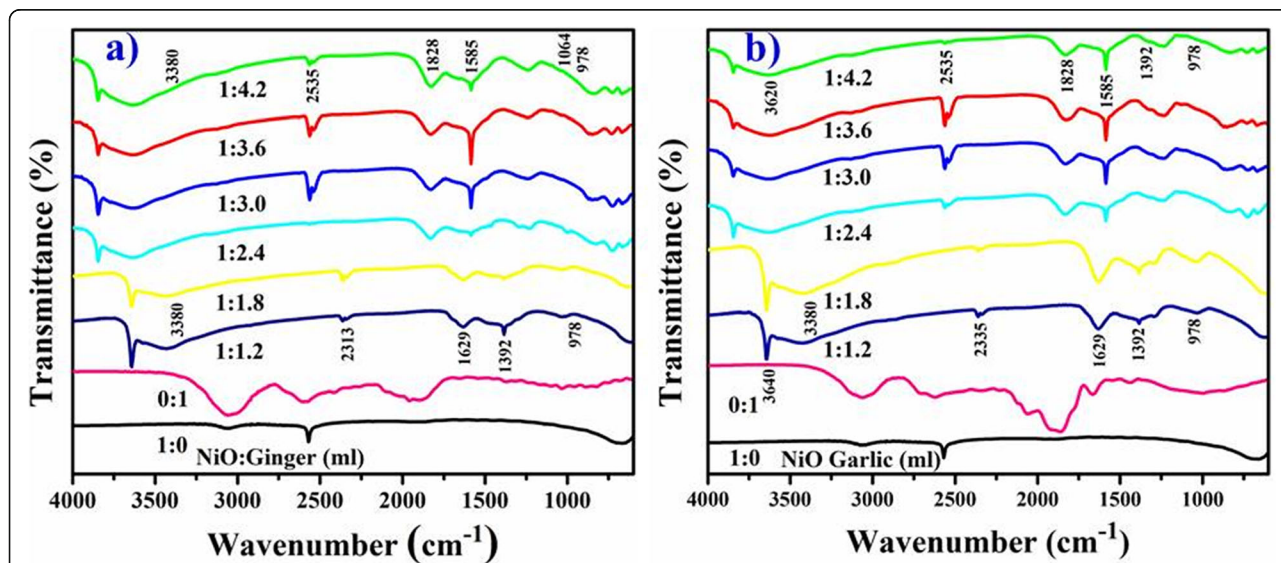


Fig. 5 FTIR spectra with ginger extract to NiO (a) and garlic (b)

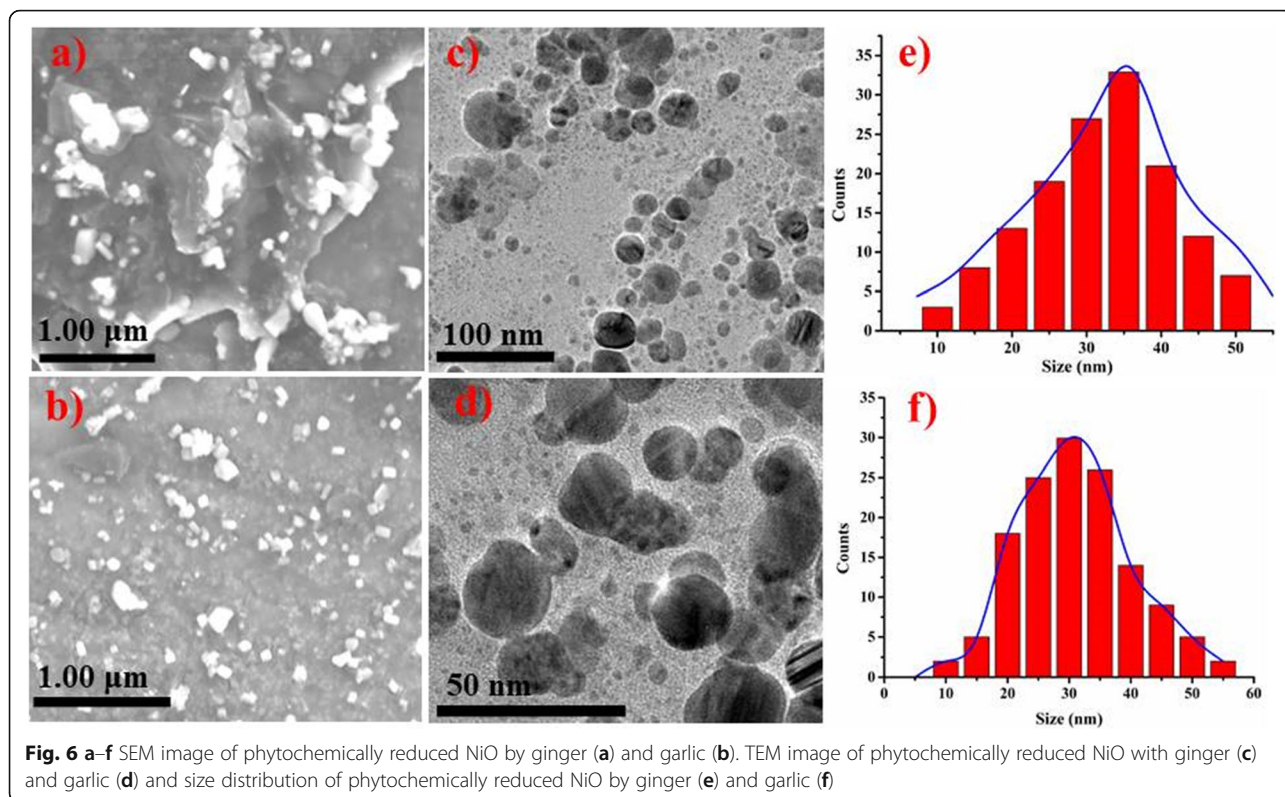


Fig. 6 a-f SEM image of phytochemically reduced NiO by ginger (a) and garlic (b). TEM image of phytochemically reduced NiO with ginger (c) and garlic (d) and size distribution of phytochemically reduced NiO by ginger (e) and garlic (f)

accompanied by blue shift. Absorption peaks of ginger and garlic extracts appeared around 275 and 280 nm, respectively. Abrupt color change in reaction mixtures was seen from wine red to light green after incorporation of root extracts. Peak broadness indicated particles agglomeration and electronic transition from valence to conduction bands with extract concentration in NiO as revealed by strong absorption bands [20]. Hence, in Fig. 3a, b results showed decrease in absorption of synthesized NPs with increasing or decreasing extract volume beyond optimized value (1:

3.6 ml). The band gap was calculated using Tauc's plot (Eq. 1).

$$(\alpha h\nu) = B(h\nu - E_g)^{1/2} \tag{1}$$

Where α is the absorption coefficient, h is the Planck's constant, B is a constant, ν is known as photon frequency, and E_g is the energy bandgap. The estimated bandgap of phytochemically reduced NiO by ginger and garlic from a plot of $(\alpha h\nu)^{1/2}$ against photon energy

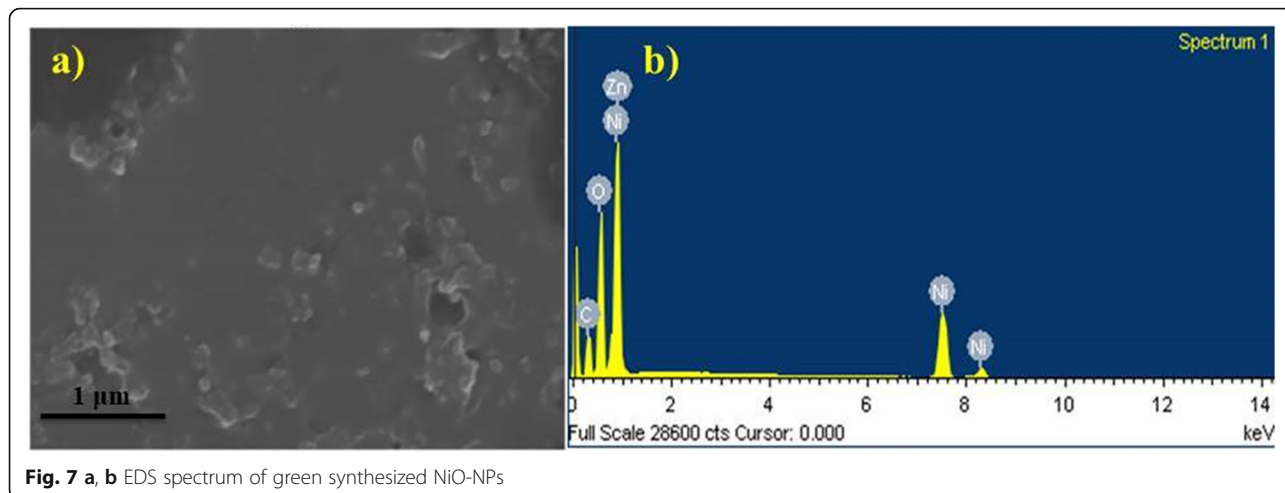


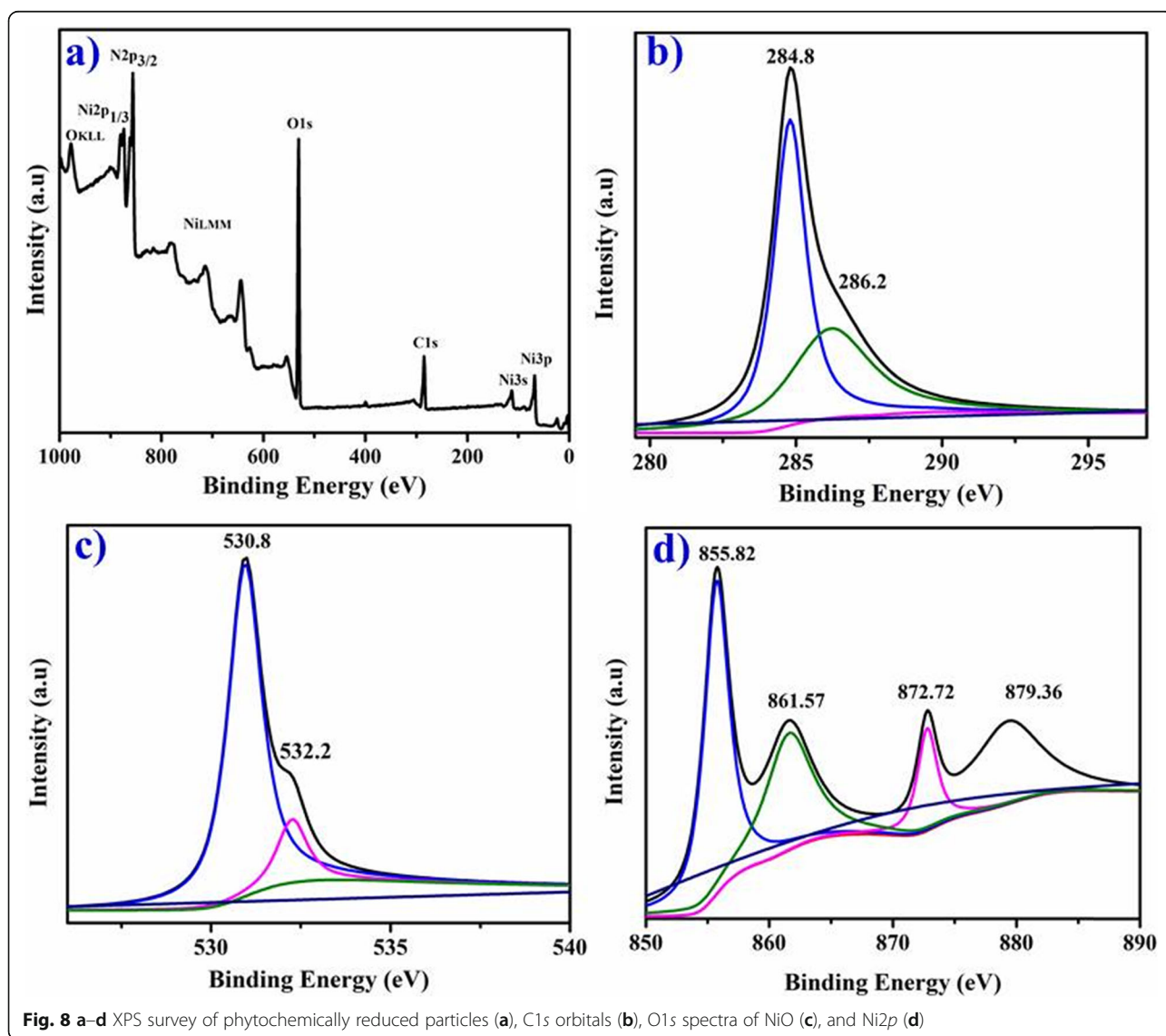
Fig. 7 a, b EDS spectrum of green synthesized NiO-NPs

(h). The intercept of a tangent to x -axis was recorded, which provides band gap energies of samples as shown in Fig. 3c, d. The variations in band gap energies were determined upon ginger doping into NiO from 4.15 to 3.1 eV and with garlic from 3.5 to 3.0 eV respectively (Fig. 3c, d).

NiO-NPs crystallinity, size, and phase composition were confirmed by XRD as shown in Fig. 4 a, b. The peaks at 2θ values 37.10° , 43.32° , 62.81° , and 76.51° correspond to (111), (200), (220), and (311) (JCPDS card no: 00-047-1049) (Fig. 4a, b) referenced by [30]. The peak intensity indicates hexagonal and face-centered cubic (fcc) NiO with average size 32.9 nm calculated by $D = 0.9\lambda/\beta\cos\theta$ for ginger and 29.92 nm for garlic phytochemically reduced NiO-NPs. The broad peaks indicate presence of oxygen spaces and local lattice disorder in sample [38]. Various phytochemicals of ginger (flavonoids, alkaloids, tannins, and saponins) and

garlic aqueous extracts (allicin, allyl sulphide, alliin, fatty acids, glycolipids, phenolics, amino acids, and flavonoids) acting as capping agents are responsible for average crystallite size of metal oxide NPs [14, 46].

The recorded FTIR spectra of NiO biosynthesized from ginger and garlic roots is shown in Fig. 5 a, b. Elaborate broad absorption at 3380 cm^{-1} correspond to OH and peak broadness indicate carbonyl group with (N-H) amine stretching frequency [50]. The sharp absorption at 2313 cm^{-1} indicates stretching vibrations of CO_2 either aerial or CO_2 inside NP grains. Rapid absorption of atmospheric CO_2 indicates greater surface area of material [18]. The broad absorption at 1629 cm^{-1} correspond to C=C aromatic ring stretching and sharp peaks at 1392 and 1064 cm^{-1} correspond to stretching vibrations of C-N aliphatic amines [48]. The intense peaks at 978 cm^{-1} confirmed metal oxygen stretching frequency of NiO [44].



The peak shifts observed after bio-reduction of NiO as 2535–2313, 1828–1629, and 1585–1392 cm^{-1} indicate phytochemicals, terpenoids, flavonoids, polyols, and proteins having ketones, alcohols, carboxylic acid, and amines functional groups responsible for chelating and capping in bio-reduction [42].

Surface morphology and size of phytochemically reduced NiO-NPs were determined using field emission scanning and transmission electron microscopy as presented in Fig. 6a–f. The NiO-NPs showed pleomorphism with cubical and more spherical shape (< 50 nm) having slight agglomeration [40]. The agglomeration of NPs could be evident from polymer adherence and magnetic interaction between the particles [49].

Elemental analysis and further features of synthesized NiO-NPs were described by energy-dispersive X-ray spectroscopy (EDS) which confirmed pure NiO phases as shown in Fig. 7a, b. The EDS spectra confirmed three peaks directly related to high purity of Ni present in tested samples between 1 and 10 kV. The atomic weight percentages observed through spectra for Ni, O, C, and Zn are 54.69, 27.81, 18.06, and – 0.55, respectively.

XPS is showing C1s, O1s, and Ni2p spectra of phytochemically reduced NiO-NPs in Fig. 8a–d that suggests chemical nature and bonding states of synthesized samples. The most intense peaks at 284.8 and 286.2 eV demonstrate C1s spectrum (Fig. 8b) corresponding to C–C and C–OH/C–O–C [21]. The O1s peak at 530.8 eV (Fig. 8c) could be assigned to hydroxyl groups of oxygen atoms, oxygen atoms adjacent to nickel vacancies, or oxygen-bounded carbon atoms C=O [1, 15, 37]. The contribution located at 532.2 eV ascribes to oxygen atoms in absorbed water molecules (NiOH) [31, 41]. The Ni2p spectrum containing Ni2p3/2 and Ni2p1/2 peaks can be separated using Gaussian–Lorentzian function into five components (Fig. 8d). The most intensive peaks at 872.72 and 855.82 eV belong to Ni2p1/2 and Ni2p3/2 with corresponding satellite peaks 879.36 and 861.57 eV, respectively [16]. The spin–orbit splitting between the Ni (2p1/2) and Ni (2p3/2) and NiO-NP core level is 17.28 eV which correspond well with earlier reports [33, 34].

The antimicrobial/bactericidal action of ginger and garlic root extracts and green/phytochemically reduced NiO-NPs was evaluated using agar well diffusion assay via inhibition zone measurement (mm) as shown in Fig. 9a–d and Table 1. The results depicted strong relation between NP concentration and inhibition zones (mm). Significant inhibition zones (mm) ($P < 0.05$) were recorded for sample 1 (1.2 ml:1), 2 (1.8 ml:1), 3 (2.4 ml:1), 4 (3 ml:1), 5 (3.6 ml:1), and 6 (4.2 ml:1) ranging (3–4.9 mm) and (3.05–5.2 mm) at low and high concentrations phytochemically reduced NiO-NPs by ginger (Fig. 9c, d), while (3.15–5.3 mm) and (3.75–5.9 mm) phytochemically reduced NPs with garlic against MDR *S. aureus* (Fig. 9e, f). Ginger root aqueous extracts depicted zero efficacy (Fig. 9a), and garlic

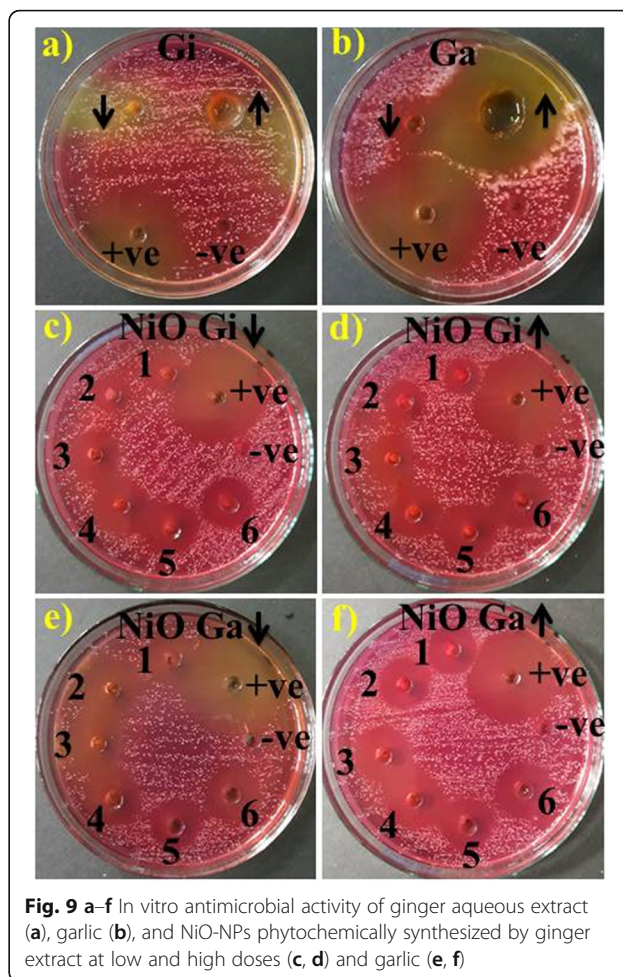


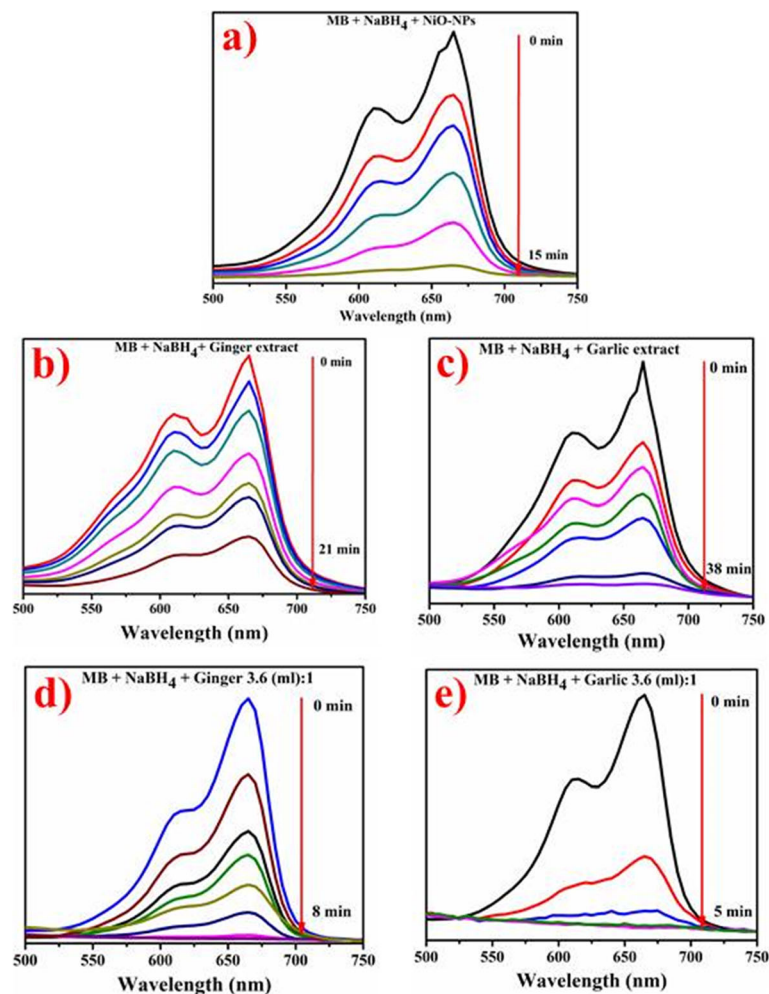
Fig. 9 a–f In vitro antimicrobial activity of ginger aqueous extract (a), garlic (b), and NiO-NPs phytochemically synthesized by ginger extract at low and high doses (c, d) and garlic (e, f)

roots showed 2.65 and 5 mm inhibition zones at low and high concentrations, respectively (Fig. 9b). All results were compared to negative control DIW (0 mm) and positive control ciprofloxacin (12.55 mm). Overall, phytochemically reduced NiO-NPs with garlic showed significant ($P < 0.05$) enhanced bactericidal action against MDR *S. aureus*.

The difference in oxidative stress tolerance depends upon various factors as surface area, morphology, and particle size of synthesized nanomaterial playing inferential role in antibacterial action potential [29, 36]. An electrostatic interaction between bacterial strains and nano-scaled materials results generation of reactive oxygen species found responsible for bacterial cell death [2–5, 22]. Two reactions found possible for nanomaterial reaction with bacterial strains including strong interaction of cations Ni^{2+} with bacterial cell negatively charged parts resulting in collapse, while second reaction results in electronic excitation from valance to conduction band upon irradiation of NiO surface with light. Further electronic reaction with O_2 generates O_2^- radicals resulting in H_2O_2 production. The $\cdot\text{OH}$ production occurred upon reaction of h^+ with water. Thus, resulting O_2^- and $\cdot\text{OH}$

Table 1 Antimicrobial activity of NiO-NPs

Microorganism	Sample	¹ Inhibition zone (mm)		² Inhibition zone (mm)	
		0.5 mg/50 μ l	1.0 mg/50 μ l	0.5 mg/50 μ l	1.0 mg/50 μ l
MDR <i>S. aureus</i>	(1.2 ml:1) 1	3	3.05	3.15	3.75
	(1.8 ml:1) 2	3.2	3.5	3.4	4.25
	(2.4 ml:1) 3	3.7	3.85	3.9	4.85
	(3.0 ml:1) 4	4.2	4.5	4.35	5.20
	(3.6 ml:1) 5	4.9	5.2	5.3	5.9
	(4.2 ml:1) 6	4.5	4.95	5	5.75
Ciprofloxacin		12.55	12.55	12.55	12.55
DIW		0	0	0	0

¹Inhibition zone of green synthesized NiO from ginger extract²Inhibition zone measurements (mm) of NPs incorporated by garlic extract**Fig. 10 a–e** Catalytic activity of NiO (a), ginger extract (b), garlic extract (c), phytochemically reduced NiO by ginger (d), and garlic reduced NPs (e)

species played significant role in breaking down of lipid or protein molecule present in bacterial cell outer surface [39].

Catalytic Activity

Figure 10 a–e demonstrating MB catalytic reduction in the presence of root extracts and green/phytochemically reduced NiO-NPs at room temperature. Figure 10 a shows catalytic potential of NiO-NPs synthesized by conventional route while (Fig. 10b, c) represents catalytic potential of ginger and garlic root aqueous extracts. Catalytic capacity of phytochemically reduced NiO-NPs is represented in Fig. 10d, e. It is obvious that NiO and plant root extracts are not an efficient nano-catalyst as they were consuming 15, 21, and 38 min for methylene blue reduction (Fig. 10a–c). Phytochemically reduced NPs with ginger showed quick degradation ($\lambda_{\max} = 8$ min) with efficient conversion of MB to leucomethylene blue (Fig. 10d). Garlic mediated NiO-NPs showed similar pattern of 100% dye reduction in 5 min (Fig. 10e).

Green/phytochemically reduced NPs perform significant catalytic dye degradation by transferring electrons from donor species (BH_4) to acceptor (MB) and stabilize system by reducing activation energy [27]. The data revealed green NPs as efficient nano-catalyst compared to conventional NPs and individual extract.

Conclusion

NiO-NPs having ginger and garlic root extracts served as excellent bactericidal as well as catalytic agent. Root extract incorporation having phytochemical groups resulted in successful NiO-NP synthesis revealed by FTIR. The XRD peaks confirmed NiO hexagonal and face-centered cubic (fcc) lattice and SEM confirmed pleomorphism with cubical and more spherical morphology of NPs having average size 16–52 (ginger doping) and 11–59 nm (garlic doping). However, elemental analysis revealed chemical nature and bonding states analyzed by EDS and XPS and presented actual percentage of nickel and oxygen, while UV analysis verified absorption peaks difference in range 350 nm and introduced blue shift at higher amount of dopants. Phytochemically garlic reduced NiO at high concentration was found more potent compared to ginger reduced NPs against MDR *S. aureus* as well as reduced MB efficiently. Thus, green/phytochemically reduced NiO from garlic root extracts may be adopted in advanced medicine as substitute of antibiotic resistance and in textile industries as catalytic agent with no environment hazard.

Abbreviations

EDS: Energy-dispersive X-ray spectroscopy; fcc: Face-centered cubic; FTIR: Fourier-transform infrared spectroscopy; G +ve: Gram positive; G –ve: Gram negative; JCPDS: Joint committee on powder diffraction standards; MB: Methylene blue; Ni: Nickel; NiO: Nickel oxide; nm: Nanometer;

NPs: Nanoparticles; SEM: Scanning electron microscopy; TEM: Transmission electron microscopy; UV-Vis: Ultra-violet visible spectroscopy; XPS: X-ray photoelectron spectroscopy; XRD: X-ray diffraction

Acknowledgements

Authors are thankful to the Higher Education Commission for financial supports via SRGP-21-1669 and CAS-TWAS President's Fellowship for international PhD students in China.

Authors' Contributions

AH and HM performed the whole experiments and wrote the manuscript. MI provided the novel idea to carry out the experiment. AH, MI, MI, JH, and IS participated in the data analysis of the results and discussion portion. JK, MMA, and SA reviewed the manuscript and corrected the English. All authors read and approved the final manuscript.

Availability of Data and Materials

All data are fully available without restriction.

Competing Interests

The authors declare that they have no competing interests.

Author details

¹Department of Clinical Medicine and Surgery, University of Veterinary and Animal Sciences, Lahore, Punjab 54000, Pakistan. ²Department of Gynaecology & Obstetric (Unit –III), Jinnah Hospital, Lahore, Punjab 54000, Pakistan. ³Tianjin Institute of Industrial Biotechnology, Chinese Academy of Sciences, 32 West 7th Avenue, Tianjin 300308, China. ⁴State key Laboratory of Chemical Resource Engineering, Beijing Advanced Innovation Centre for Soft Matter Science and Engineering, Beijing Engineering Center for Hierarchical Catalysts, Beijing University of Chemical Technology, Beijing 100029, China. ⁵Department of Food Sciences, Cholistan University of Veterinary and Animal Sciences, Near DHA663100, Bahawalpur, Pakistan. ⁶University College of Pharmacy, University of the Punjab, Lahore 54000, Pakistan. ⁷Institute of Biochemistry and Biotechnology, University of Veterinary and animal sciences, Lahore, Punjab 54000, Pakistan. ⁸Solar Cell Applications Research Lab, Department of Physics, Government College University, Lahore, Punjab 54000, Pakistan.

Received: 11 November 2019 Accepted: 18 February 2020

Published online: 02 March 2020

References

1. Abu-Zied BM, Asiri AM (2014) An investigation of the thermal decomposition of silver acetate as a precursor for nano-sized Ag-catalyst. *Thermochim Acta* 581:110–117
2. Ahmed B, Hashmi A, Khan MS, Musarrat J (2018) ROS mediated destruction of cell membrane, growth and biofilms of human bacterial pathogens by stable metallic AgNPs functionalized from bell pepper extract and quercetin. *Adv Powder Technol* 29(7):1601–1616
3. Ahmed B, Solanki B, Zaidi A, Khan MS, Musarrat J (2019) Bacterial toxicity of biomimetic green zinc oxide nanoantibiotic: insights into ZnONP uptake and nanocolloid–bacteria interface. *Toxicology research* 8(2):246–261
4. Ali K, Ahmed B, Ansari SM, Saquib Q, Al-Khedhairi AA, Dwivedi S, Alshaeri M, Khan MS, Musarrat J (2019) Comparative in situ ROS mediated killing of bacteria with bulk analogue, eucalyptus leaf extract (ELE)-capped and bare surface copper oxide nanoparticles. *Mater Sci Eng C* 100:747–758
5. Ali K, Ahmed B, Khan MS, Musarrat J (2018) Differential surface contact killing of pristine and low EPS *Pseudomonas aeruginosa* with Aloe vera capped hematite ($\alpha\text{-Fe}_2\text{O}_3$) nanoparticles. *J Photochem Photobiol B Biol* 188:146–158
6. Ali S, Superkar P, Shukla P (1989) A study of incidence of subclinical mastitis (SCM) in cows in Mhow region. *Gujrat Vet* 16:16–28
7. Altaf M, Ijaz M, Ghaffar A, Rehman A, Avais M (2019) Antibiotic susceptibility profile and synergistic effect of non-steroidal anti-inflammatory drugs on antibacterial activity of resistant antibiotics (Oxytetracycline and Gentamicin) against methicillin resistant *Staphylococcus aureus* (MRSA). *Microb Pathog* 137:103755
8. Angajala G, Radhakrishnan S (2014) A review on nickel nanoparticles as effective therapeutic agents for inflammation. *Inflammation and Cell Signaling* 1(3):1–8

9. Balati A, Bazilio A, Shahriar A, Nash K, Shipley HJ (2019a) Simultaneous formation of ultra-thin MoSe₂ nanosheets, inorganic fullerene-like MoSe₂ and MoO₃ quantum dots using fast and ecofriendly pulsed laser ablation in liquid followed by microwave treatment. *Mater Sci Semicond Process* 99:68–77
10. Balati A, Tek S, Nash K, Shipley H (2019b) Nanoarchitecture of TiO₂ microspheres with expanded lattice interlayers and its heterojunction to the laser modified black TiO₂ using pulsed laser ablation in liquid with improved photocatalytic performance under visible light irradiation. *J Colloid Interface Sci* 541:234–248
11. Balati A, Wagle D, Nash KL, Shipley HJ (2019c) Heterojunction of TiO₂ nanoparticle embedded into ZSM5 to 2D and 3D layered-structures of MoS₂ nanosheets fabricated by pulsed laser ablation and microwave technique in deionized water: structurally enhanced photocatalytic performance. *Appl Nanosci* 9(1):19–32
12. Banerjee S, Mullick H, Banerjee J, Ghosh A (2011) Zingiber officinale: a natural gold. *Int J Pharmaceutical Bio-Sci* 2:283–294
13. Behera S, Ojha A, Rout J, Nayak P (2012) Plant mediated synthesis of silver nanoparticles: opportunity and challenge. *International Journal of Biology Pharmacy and Allied Sciences* 1(11):1637–1658
14. Bhandari PR (2012) Garlic (*Allium sativum* L.): A review of potential therapeutic applications. *International Journal of Green Pharmacy (IJGP)* 6:2
15. Biesinger MC, Payne BP, Lau LW, Gerson A, Smart RSC (2009) X-ray photoelectron spectroscopic chemical state quantification of mixed nickel metal, oxide and hydroxide systems. *Surface and Interface Analysis: An International Journal devoted to the development and application of techniques for the analysis of surfaces, interfaces and thin films* 41(4):324–332
16. Biju V (2007) Ni 2p X-ray photoelectron spectroscopy study of nanostructured nickel oxide. *Mater Res Bull* 42(5):791–796
17. Cao G, Wang Y (2004) Nanostructures and nanomaterials: synthesis. *Properties and Applications* 2
18. Chen Z, Shi E, Li W, Zheng Y, Wu N, Zhong W (2002) Particle size comparison of hydrothermally synthesized cobalt and zinc aluminate spinels. *J Am Ceram Soc* 85(12):2949–2955
19. Dodd F (1983) Mastitis—progress on control. *J Dairy Sci* 66(8):1773–1780
20. Endres J, Egger DA, Kulbak M, Kerner RA, Zhao L, Silver SH, Hodes G, Rand BP, Cahen D, Kronik L (2016) Valence and conduction band densities of states of metal halide perovskites: a combined experimental–theoretical study. *The journal of physical chemistry letters* 7(14):2722–2729
21. Furlan A, Lu J, Hultman L, Jansson U, Magnuson M (2014) Crystallization characteristics and chemical bonding properties of nickel carbide thin film nanocomposites. *J Phys Condens Matter* 26(41):415501
22. Haroon M, Zaidi A, Ahmed B, Rizvi A, Khan MS, Musarrat J (2019) Effective inhibition of phytopathogenic microbes by eco-friendly leaf extract mediated silver nanoparticles (AgNPs). *Indian J Microbiol* 59(3):273–287
23. Hawkey P. 2008. The growing burden of antimicrobial resistance. *Journal of antimicrobial chemotherapy*. 62(suppl_1): i1–i9.
24. Hernawan UE, SETYAWAN AD (2003) Organosulphure compound of garlic (*Allium sativum* L.) and its biological activities. *Biofarmasi Journal of Natural Product Biochemistry* 1(2):65–76
25. Hinckley L, Benson R, Post J (1987) How management affects the control of staphylococcal mastitis. *Veterinary medicine (USA)*
26. Hyeon T. 2003. Chemical synthesis of magnetic nanoparticles. *Chemical Communications*. (8): 927–934.
27. Indana MK, Gangapuram BR, Dadigala R, Bandi R, Guttena V (2016) A novel green synthesis and characterization of silver nanoparticles using gum tragacanth and evaluation of their potential catalytic reduction activities with methylene blue and Congo red dyes. *Journal of Analytical Science and Technology* 7(1):19
28. Iwalokun B, Ogunledun A, Ogbolu D, Bamiro S and Jimi-Omojola J (2004) In vitro antimicrobial properties of aqueous garlic extract against multidrug-resistant bacteria and *Candida* species from Nigeria. *Journal of medicinal food* 7(3):327–333.
29. Jesudoss S, Judith Vijaya J, John Kennedy L, Iyyappa RP, Al-Lohedan HA, Jothi Ramalingam R, Kaviyarasu K, Bououdina M (2016) Studies on the efficient dual performance of Mn_{1-x}Ni_xFe₂O₄ spinel nanoparticles in photodegradation and antibacterial activity. *J Photochem Photobiol B Biol* 165:121–132
30. Kganyago P, Mahlale-Glory L, Mathipa M, Ntsendwana B, Mketi N, Mbita Z, Hintscho-Mbita N (2018) Synthesis of NiO nanoparticles via a green route using *Monsonia burkeana*: the physical and biological properties. *J Photochem Photobiol B Biol* 182:18–26
31. Kim S-I, Lee J-S, Ahn H-J, Song H-K, Kang J-H (2013) Facile route to an efficient NiO supercapacitor with a three-dimensional nanonetwork morphology. *ACS Appl Mater Interfaces* 5(5):1596–1603
32. Komolafe O (2003) Antibiotic resistance in bacteria—an emerging public health problem. *Malawi Med J* 15(2):63–67
33. Kumar H, Ghosh S, Avasthi D, Kabiraj D, Lalla N, Shripathi T, Pivin J (2010) Magnetic and field emission studies of atom beam sputtered Ni: SiO₂ granular films. *Vacuum*. 85(2):139–144
34. Lenglet M, Hochu F, Dürr J, Tuilier M (1997) Investigation of the chemical bonding in 3d8 nickel (II) charge transfer insulators (NiO, oxidic spinels) from ligand-field spectroscopy, Ni 2p XPS and X-ray absorption spectroscopy. *Solid State Commun* 104(12):793–798
35. Mariam AA, Kashif M, Arokiyaraj S, Bououdina M, Sankaracharyulu M, Jayachandran M, Hashim U (2014) Bio-synthesis of NiO and Ni nanoparticles and their characterization. *Digest Journal of Nanomaterials and Biostructures* 9(3):1007–1019
36. Navale GR, Rout CS, Gohil KN, Dharm MS, Late DJ, Shinde SS (2015) Oxidative and membrane stress-mediated antibacterial activity of ws 2 and rgo-ws 2 nanosheets. *RSC Adv* 5(91):74726–74733
37. Payne B, Biesinger M, McIntyre N (2012) Use of oxygen/nickel ratios in the XPS characterisation of oxide phases on nickel metal and nickel alloy surfaces. *J Electron Spectrosc Relat Phenom* 185(5-7):159–166
38. Prabhu YT, Rao KV, Kumar VSS, Kumari BS (2013) Synthesis of ZnO nanoparticles by a novel surfactant assisted amine combustion method. *Advances in Nanoparticles* 2(01):45
39. Rajan PI, Vijaya JJ, Jesudoss S, Kaviyarasu K, Kennedy LJ, Jothiramalingam R, Al-Lohedan HA, Vaali-Mohammed M-A (2017) Green-fuel-mediated synthesis of self-assembled NiO nano-sticks for dual applications—photocatalytic activity on Rose Bengal dye and antimicrobial action on bacterial strains. *Materials Research Express* 4(8):085030
40. Saleem S, Ahmed B, Khan MS, Al-Shaeri M, Musarrat J (2017) Inhibition of growth and biofilm formation of clinical bacterial isolates by NiO nanoparticles synthesized from eucalyptus globulus plants. *Microb Pathog* 111:375–387
41. Salvati L Jr, Makovsky LE, Stencil J, Brown F, Hercules DM (1981) Surface spectroscopic study of tungsten-alumina catalysts using X-ray photoelectron, ion scattering, and Raman spectroscopies. *J Phys Chem* 85(24):3700–3707
42. Shankar SS, Rai A, Ahmad A, Sastry M (2004) Rapid synthesis of Au, Ag, and bimetallic Au core–Ag shell nanoparticles using Neem (*Azadirachta indica*) leaf broth. *J Colloid Interface Sci* 275(2):496–502
43. Singh C, Sharma V, Naik PK, KHandelwal V, Singh H (2011) A green biogenic approach for synthesis of gold and silver nanoparticles using Zingiber officinale. *Digest Journal of Nanomaterials and Biostructures* 6(2):535–542
44. Suresh S, Saravanan P, Jayamoorthy K, Kumar SA, Karthikeyan S (2016) Development of silane grafted ZnO core shell nanoparticles loaded diglycidyl epoxy nanocomposites film for antimicrobial applications. *Mater Sci Eng C* 64:286–292
45. Thema F, Manikandan E, Gurib-Fakim A, Maaza M (2016) Single phase Bunsenite NiO nanoparticles green synthesis by *Agathosma betulina* natural extract. *J Alloys Compd* 657:655–661
46. Tsiaganis MC, Laskari K, Melissari E (2006) Fatty acid composition of *Allium* species lipids. *J Food Compos Anal* 19(6-7):620–627
47. Vidya C, Hiremath S, Chandraprabha M, Antonyraj ML, Gopal IV, Jain A, Bansal K (2013) Green synthesis of ZnO nanoparticles by *Calotropis gigantea*. *Int J Curr Eng Technol* 1:118–120
48. Wang T, Jin X, Chen Z, Megharaj M, Naidu R (2014) Green synthesis of Fe nanoparticles using eucalyptus leaf extracts for treatment of eutrophic wastewater. *Sci Total Environ* 466:210–213
49. Wang XS, Liu X, Wen L, Zhou Y, Jiang Y, Li Z (2008) Comparison of basic dye crystal violet removal from aqueous solution by low-cost biosorbents. *Sep Sci Technol* 43(14):3712–3731
50. Xia X, Tu J, Zhang J, Wang X, Zhang W, Huang H (2008) Electrochromic properties of porous NiO thin films prepared by a chemical bath deposition. *Sol Energy Mater Sol Cells* 92(6):628–633

Publisher's Note

Springer Nature remains neutral with regard to jurisdictional claims in published maps and institutional affiliations.